Noname manuscript No.
(will be inserted by the editor)

Pedicle Screw Navigation using Surface Digitization on the Microsoft HoloLens

Florentin Liebmann[1,2] · Simon Roner[1,3] · Marco von Atzigen[1] · Davide Scaramuzza[4,5] · Reto Sutter[6] · Jess Snedeker[2,3] · Mazda Farshad[3] · Philipp Fürnstahl[1]

[1]Computer Assisted Research and Development Group, Balgrist University Hospital, University of Zurich, Zurich, Switzerland
[2]Laboratory for Orthopaedic Biomechanics, ETH Zurich, Zurich, Switzerland
[3]Orthopaedic Department, Balgrist University Hospital, University of Zurich, Zurich, Switzerland
[4]Department of Informatics, University of Zurich, Zurich, Switzerland
[5]Department of Neuroinformatics, University of Zurich and ETH Zurich, Zurich, Switzerland
[6]Radiology Department, Balgrist University Hospital, University of Zurich, Zurich, Switzerland

Received: date / Accepted: date

Abstract
Purpose: In spinal fusion surgery, imprecise placement of pedicle screws can result in poor surgical outcome or may seriously harm a patient. Patient-specific instruments and optical system have been proposed for improving precision through surgical navigation compared to free-hand insertion. However, existing solutions are expensive and cannot provide in situ visualizations. Recent technological advancement enabled the production of more powerful and precise optical see-through head-mounted displays for the mass market. The purpose of this laboratory study was to evaluate whether such a device is sufficiently precise for the navigation of lumbar pedicle screw placement.

Methods: A novel navigation method, tailored to run on the Microsoft HoloLens, was developed. It comprises capturing of the intraoperatively reachable surface of vertebrae to achieve registration and tool tracking with real-time visualizations without the need of intraoperative imaging. For both, surface sampling and navigation, 3D printable parts, equipped with fiducial markers, were employed. Accuracy was evaluated within a self-built setup based on two phantoms of the lumbar spine. Computed Tomography (CT) scans of the phantoms were acquired to carry out preoperative planning of screw trajectories in 3D. A surgeon placed

Florentin Liebmann
Balgrist University Hospital
Forchstrasse 340
8008 Zurich
Switzerland
Tel.: +41 44 510 73 59
E-mail: florentin.liebmann@balgrist.ch

the guiding wire for the pedicle screw bilaterally on ten vertebrae guided by the navigation method. Postoperative CT scans were acquired to compare trajectory orientation (3D angle) and screw insertion points (3D distance) with respect to the planning.
Results: The mean errors between planned and executed screw insertion were $3.38 \pm 1.73^{\circ}$ for the screw trajectory orientation and 2.77 ± 1.46 mm for the insertion points. The mean time required for surface digitization was 125 ± 27 s.
Conclusions: First promising results under laboratory conditions indicate that precise lumbar pedicle screw insertion can be achieved by combining HoloLens with our proposed navigation method. As a next step, cadaver experiments need to be performed to confirm the precision on real patient anatomy.

Keywords Surgical navigation · Augmented reality · Surface digitization · HoloLens · Spine · Pedicle screw

1 Introduction

Spine disorders are among the most frequent musculoskeletal pathologies in developed countries [1]. They cause diminished quality-of-life to the patients and result in substantial socio-economical costs [2]. Most patients can be treated successfully in a conservative way by initial physical protection, pain medication and back training [3]. However, surgery is indicated in patients with more severe conditions such as degenerative disc disease, fracture treatment, and scoliosis. In such pathologies, spinal fusion has been established as the benchmark surgical treatment [4–6].

In the state-of-the-art surgical treatment an open surgery is performed, in which the vertebrae of the pathological segment are fused with an orthopaedic implant. Pedicle screws are drilled into each vertebra and connected with the implant to achieve a rigid connection of the bone-implant interface. Screw insertion relies on the preparation of guiding holes with a surgical awl or by drilling K-wires. The surgeon aims for a central position of the guiding hole within the pedicle by using bony landmarks as an orientation help. Deviation from the optimal position can result in pedicle screw penetration which in turn can lead to serious injury of the spinal cord, nerve roots, and major vessels.

Unfortunately, accuracy of placement of pedicle screws is low with 68% with use of the standard method by aid of conventional fluoroscopy [7]. In more challenging scenarios, such as instrumentation of neuromuscular scoliosis, the accuracy is even less, particularly in the upper thoracic region [8]. 3D printing techniques have been proposed to increase accuracy [9, 10]. However, manufacturing is time consuming and expensive. Furthermore, the lack of intraoperative flexibility is considered to be disadvantageous. More popular navigation approaches are based on imaging. 2D and 3D fluoroscopic navigation can increase accuracy to 84% and 96%, respectively [7]. Wile 2D/3D fluoroscopy provide surgical navigation in a passive way, intraoperative CT can be used in combination with high-end optical or even robotic navigation systems [11] to enable real-time tool and screw localization. However, the increased use of fluoroscopy or CT exposes the patient to a significant amount of radiation [12–15].

Several methods have been proposed to avoid the use of intraoperative imaging. In intraoperative manual surface digitization approaches, part of the intraoperative bone anatomy is acquired by optically-tracked pointing devices [16–18]. The so acquired bone surface can be registered to the preoperative planning using surface registration algorithms [16]. Combined with tool tracking, these methods can provide real-time surgical navigation displayed

on wall- or rack-mounted 2D monitors [19]. Despite the interesting and easy to use registration approach, these systems are prone to occlusion problems because they cannot provide in situ image acquisition and visualization [20]. In addition, they come along with high costs for acquisition and maintenance.

A simpler and cheaper system to increase precision of pedicle screw placement would be favorable. One solution could be the application of augmented reality (AR). AR technology is capable of superimposing a preoperative planning with the intraoperative anatomy such that surgical navigation can be provided directly in the line of sight of a surgeon. In the medical context, AR aroused interest already several decades ago [21] but the implementation into surgical practice remains very limited [22]. Recent technological advancement enabled the production of more computational powerful and more precise optical see-through head-mounted displays (OST-HMD) for the mass market. In [23], an OST-HMD based navigation solution for pedicle screws has been proposed. However, as the registration relies on an external ultrasound device for anatomy acquisition, the setup can be considered to be complex.

Based on the Microsoft HoloLens (Microsoft Corporation, Redmond, WA, USA), an off-the-shelf OST-HMD of latest technology, we propose a radiation-free surgical navigation approach comprising intraoperative manual surface digitization and intuitive holographic navigation. The goal of this study was to investigate whether our approach is sufficiently precise for enabling AR-navigated insertion of lumbar pedicle screws. Precision was evaluated within a laboratory experiment in which the surgical procedure was performed on phantoms.

2 Methods

The presented method consists of three main components: marker tracking and pose estimation, intraoperative surface digitization for registration and surgical navigation. Each component as well as the experimental setup and design will be explained hereafter.

2.1 Marker tracking and pose estimation

The two main steps performed intraoperatively are registration and navigation. Both rely on marker tracking. Marker tracking was implemented employing the two front-facing of the four environment tracking cameras of the HoloLens that are accessible via Research Mode [24]. We fielded commercially available, sterile fiducial markers (Clear Guide Medical, Baltimore MD, USA). Their patterns originate from the AprilTags library [25, 26]. Before describing the method in detail, we provide some required background on the different coordinate systems of the HoloLens [27] which are illustrated in Figure 1.

App-specified Coordinate System (ASCS): a fixed reference coordinate system of the HoloLens in the real world, defined on application startup.

HoloLens Coordinate System (HCS): the coordinate system which is fixed to the HoloLens. All sensor spaces can be described relative to this coordinate system.

3D Camera View Space (CVS): the space with origin in the camera center, CVSL for the left and CVSR for the right camera.

2D Camera Projection Space (CPS): the space of normalized image coordinates (-1 to 1 in both the X and Y axis) with respect to a camera. CPSL and CPSR denote the left and right camera space, respectively.

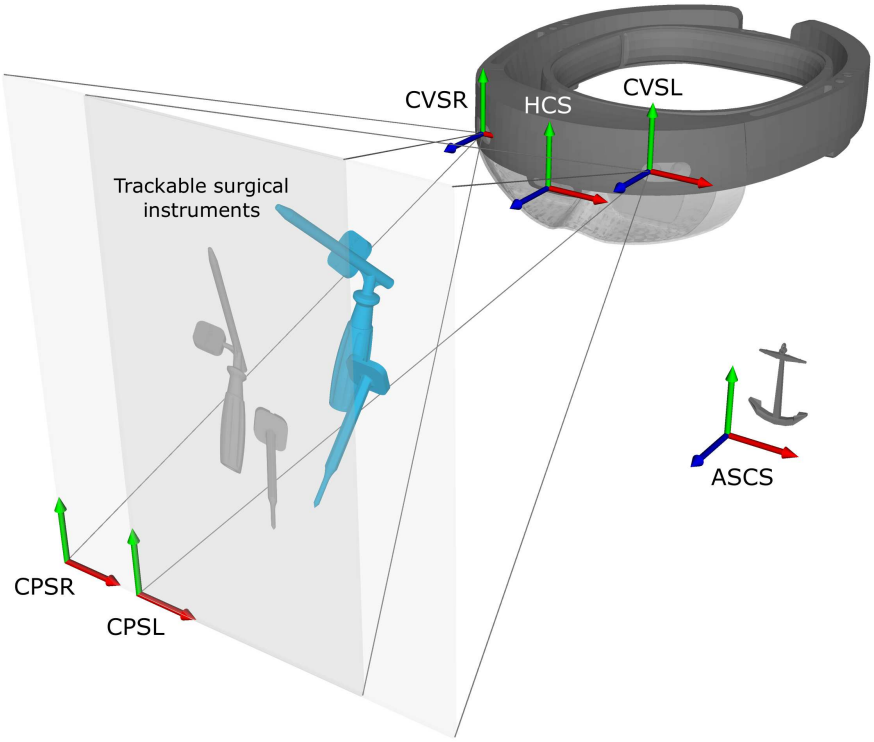

Fig. 1: Exemplary illustration of the HoloLens' coordinate systems used: App-specified Coordinate System (ASCS), HoloLens Coordinate System (HCS), 3D Camera View Space (CVS, left and right) and 2D Camera Projection Space (CPS, left and right). The HoloLens 3D model originates from "Free Hololens Model + Textures" by EdgeFlow Studio and the anchor 3D model from "Medieval Anchor" by wolfgar74. Both are licensed under CC BY 4.0.

An exemplary transformation from CPS to CVS is denoted as T_{CPS}^{CVS}. For each pair of images (left and right) with a detectable marker, its pose was derived as follows. Initial estimate values $C_1^L,\ldots,C_4^L$ and $C_1^R,\ldots,C_4^R$ of the four corners of the marker are detected in both images using standard detection method [28–30]. Due to the poor resolution (480x640 pixels) of the environmental cameras, each C_i was passed to a dedicated Kalman filter [31, 32]. We integrated a constant velocity model in the filters, because movements of the surgeon between consecutive frames can be considered as constant given the high rate of 30 frames per second. A process noise covariance of 1×10^{-5} was assumed in the prediction step of the filter. The measurement noise 1×10^{-4} of the update step was determined heuristically from experimental data in which both estimated and ground truth marker corners were known.

The filtered corner estimates were transformed to CPS and extended by one dimension (unit plane: $z=1$) such that they can be expressed in CVS and further transformed to HCS. In order to perform triangulation, directional vectors $\mathbf{d}_i^L$ and $\mathbf{d}_i^R$ between each $T_{CPSL}^{HCS}C_i^L$ and $T_{CPSR}^{HCS}C_i^R$ and their respective camera centers have to be formed. The triangulation can be completed by finding the closest point $min(\mathbf{d}_i^L,\mathbf{d}_i^R)$ between each pair of directional vectors.

Given the new 3D estimates $min(\mathbf{d}_i^L, \mathbf{d}_i^R)$, the 3D marker pose can be derived by incorporating prior knowledge about the marker geometry. As the true 3D position gt_i of each corner point with respect to the marker center is known, the 3D pose estimation problem can be reduced to the problem of finding a rigid transformation between the point pairs $min(\mathbf{d}_i^L, \mathbf{d}_i^R)$ and gt_i in a least-square sense. The transformation is calculated by applying the absolute orientation [33].

2.2 Registration

The key idea of our intraoperative surface digitization approach is the establishment of a correspondence between pre- and intra-operative anatomy without needing intraoperative imaging.

For each vertebra a sparse point cloud of relevant bone surface regions is collected by the surgeon in the surgery. A custom-made pointing device (PD), as illustrated in Figure 2a, is used for performing surface acquisition. The PD consists of a notch, a handle and tip. The tip is tapered in a way such that points can be reached at different angles without introducing an offset. The notch can be mounted with sterile fiducial markers such as the ones described in Section 2.1. Due to the known geometry of the PD, it is straightforward to extrapolate from the marker pose to the position of the tip.

(a) (b) (c) (d)

Fig. 2: a) The pointing device. b) A surgeon wearing the HoloLens uses the pointing device in the experimental setup. c) The augmented view of the surgeon during surface sampling. d) Overlay of vertebra L1 after registration (insertion points are denoted in blue).

After application startup, the surgeon is asked to sample accessible surface regions of the vertebra (see Figure 2b) in a specific pattern which was trained previously. To do so, the PD is moved along the anatomy while pressing down the button of the HoloLens clicker [34] (events implemented in MixedRealityToolkit-Unity [35]). For each camera frame the marker tracking method of Section 2.1 is applied and the 3D tip position is recorded, as long as the button remains pressed. Sampled areas are visualized by a thin line connecting consecutively collected points (see Figure 2c). Once the button is released, a voice command (events implemented in MixedRealityToolkit-Unity [35]) can be used to indicate whether a collected region should be saved (“save”) or discarded (“delete”). Only the saved points

were used in the registration process. When sufficient points have been sampled, the surgeon initiates registration by a double click.

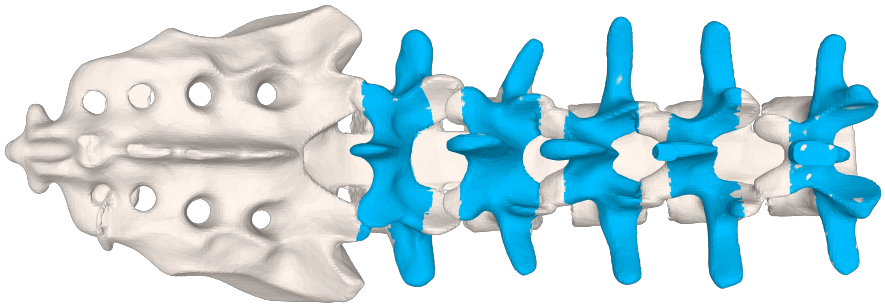

Fig. 3: Template for the bone surface of spine segments L1 - L5 that is assumed to be accessible intraoperatively (colored areas). The template was constructed by a surgeon.

The intraoperatively collected point cloud pc_{intra} is registered to the point cloud pc_{pre} representing the points of the 3D model of the preoperative vertebra. pc_{pre} has been obtained from the 3D triangular surface model (herein after called 3D model) of the segmented preoperative CT scan (see Section 2.4). In a preprocessing step, pc_{pre} is trimmed by removing points which can definitely not be reached with the PD in a surgery. The points are identified by using a template model which encodes intraoperatively accessible regions (see Figure 3).

The registration process works in a fully automated fashion and comprising three steps: coarse registration, iterative closest point (ICP) based fine registration [36], and result selection. Coarse registration is achieved by identifying three corresponding extremal points in each of the point clouds. To this end, a principle component analysis (PCA) [37], implemented in ALGLIB (ALGLIB Project, Nizhny Novgorod, Russia), is performed on pc_{intra}, yielding the respective principle axes pa_1^{intra}, pa_2^{intra} and pa_3^{intra} ordered by decreasing magnitude. The three extremal points e_1^{intra}, e_2^{intra} and e_3^{intra} are determined using the dot product as follows:

$$
\begin{aligned}
e_1^{intra} &= max(pa_1^{intra} \cdot p_i, p_i \in pc_{intra}) \\
e_2^{intra} &= min(pa_1^{intra} \cdot p_i, p_i \in pc_{intra}) \\
e_3^{intra} &= max(abs(pa_2^{intra} \cdot p_i, p_i \in pc_{intra}))
\end{aligned}
$$

Correspondingly, the extrema points e_1^{pre}, e_2^{pre} and e_3^{pre} are calculated. Due to the symmetry of the vertebra along pa_1, two possible coarse registration configurations must be evaluated (see Figures 4a and 4b) and considered for the fine registration by applying absolute orientation [33] to both point pair sets.

$$
\begin{aligned}
&\{(e_1^{intra}, e_1^{pre})\}, \{(e_2^{intra}, e_2^{pre})\}, \{(e_3^{intra}, e_3^{pre})\} \\
&\{(e_1^{intra}, e_2^{pre})\}, \{(e_2^{intra}, e_1^{pre})\}, \{(e_3^{intra}, e_3^{pre})\}
\end{aligned}
$$

Afterwards, fine registration is performed using ICP on both configurations. Thereby, the algorithm is terminated when either the number of iterations exceeds 50 or the difference in

root mean squared error (RMSE) between two steps remains below 10^{-7}. Lastly, the RMSE is evaluated for each registered configuration and the one with the smallest RMSE is selected (Figure 4c). The final result is shown to the surgeon by superimposing the preoperative 3D model with the intraoperative anatomy (see Figure 2d). This gives the surgeon the possibility to verify the registration by visual inspection. If the result is satisfactory, surgical navigation can be started by another double click.

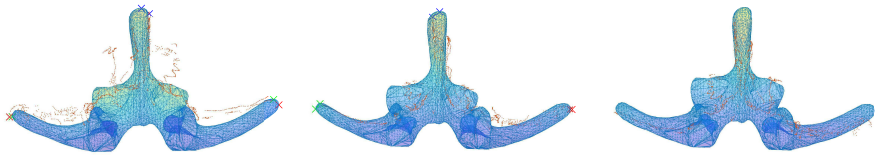

(a) (b) (c)

Fig. 4: pc_{pre} denotes the points of the 3D model. pc_{intra} is shown in orange. The red, green and blue crosses in a) and b) represent the respective extremal points used for coarse alignment. a) Incorrect coarse alignment. b) Correct coarse alignment. c) The fine alignment resulting from b).

2.3 Surgical navigation

The surgical navigation approach relies on a trackable custom-made navigation device (ND), illustrated in Figure 5a. Handle and sleeve are designed in such a way that they allow holding the ND with one hand, while inserting a K-wire with the other (Figure 5b). Simultaneously, by detecting the integrated marker, the current tip position and trajectory orientation are measured and evaluated with the marker tracking component of Section 2.1.

When navigation starts, the 3D model of the vertebra is hidden and only the screws' entry points are shown (blue in Figure 5c). The surgeon mounts the K-wire into the drill and threads it through the sleeve of the ND. The pointed tip of the K-wire can then be used to pierce a small hole into the bone at the position of the targeted entry point, purely relying on the holographic visualization. After doing so, the K-wire tip cannot slide away anymore and the surgeon can start to navigate towards the desired trajectory. Thereby, holographic feedback comprises two parts of information. First, the 3D angle between current and targeted trajectory is displayed (see Figure 5d). Second, a triangle is rendered between three virtual points: the screw entry point (A in Figure 5d), a point lying on the current trajectory of the ND (B in Figure 5d) and one lying on the targeted screw trajectory (C in Figure 5d). The intention of the triangle was to give the surgeon an intuitive feedback about the trajectory deviation in 3D space. A red triangle means the current trajectory passes an area that must be avoided. Yellow means not perfect, but still acceptable, and green means the angle is less than 5°. Once the surgeon has aligned the current trajectory with the one of the preoperative plan, the K-wire can be drilled into the pedicle.

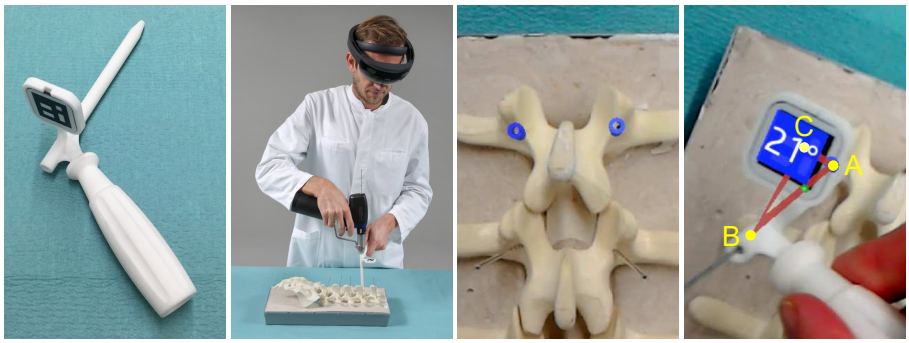

(a) (b) (c) (d)

Fig. 5: a) The custom-made navigation device. b) The surgeon uses the navigation device in the experimental setup. c) Entry point overlay in the beginning of the navigation (entry points are shown in blue). d) Augmented view of the surgeon during navigation. The number represents the 3D angle between current and targeted screw trajectory. A, B and C (not visible in the augmented view) denote entry point, a point lying on the current trajectory and one lying on the targeted screw trajectory. They form a colored triangle (red) and serve as intuitive feedback about the trajectory deviation in 3D space.

2.4 Evaluation and experimental setup

Our method was evaluated on two phantoms of the lower lumbar spine (Synbone AG, Zizers, Switzerland) consisting of L1 – L5. The phantoms feature also facet joints and discs such that a more realistic inter-vertebral movement can be achieved. The phantoms were CT scanned according to a clinical protocol (120 kV; 1 mm slice thickness; 0.5 mm slice increment; Brilliance 40 CT, Philips Healthcare, Best, The Netherlands) and 3D models were generated by applying global thresholding and region growing with the Mimics software (version 19.0, Materialise NV, Leuven, Belgium). Preoperative planning and surgical execution was performed by a senior resident surgeon with experience in surgical navigation.

Preoperative planning was carried using the preoperative planning software CASPA (version 5.26, Balgrist CARD AG, Zurich, Switzerland). For each vertebra, two screw trajectories were placed in the centers of the pedicles, maximizing the margins to the bone cortex. The orientations of the trajectories were defined based on landmarks on the posterior arc (see Figure 6a).

The phantoms were molded into a plastic tub using plaster to ensure that only those parts of the vertebral bodies, which can be also accessed through the surgery, will be visible in the experiment.

The preoperative plan was then executed following the workflow of our method. Each vertebra was registered individually and two K-wires (left, right) were inserted, solely relying on AR navigation. This process was performed for each of the two phantoms. After execution, postoperative CT scans were acquired from which 3D models of the vertebrae were generated using the segmentation functionality of Mimics. In contrast to the preoperative data, manual segmentation of the K-wires and metal artifact removal had to be performed (see Figure 6b). The postoperative 3D models were aligned to the preoperative plan following a clinically established method used for pre-post evaluations [38, 39]. For each postoperative K-wire, trajectory and entry point were quantified. The trajectory was defined

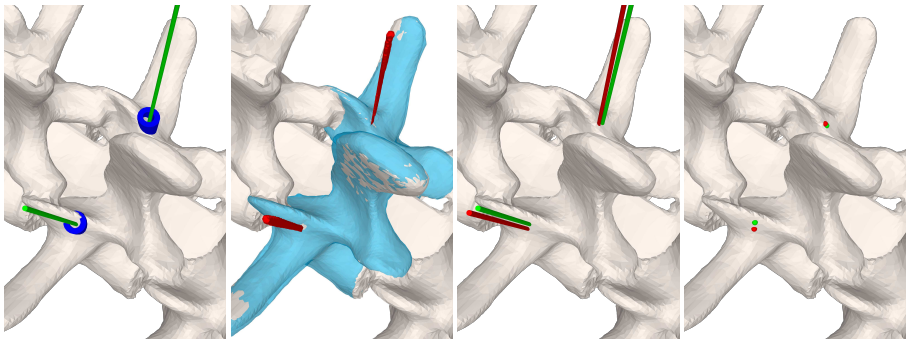

(a) (b) (c) (d)

Fig. 6: a) Preoperatively planned trajectories on spine segment L3. b) Postoperatively segmented 3D models of spine segment 3 and inserted K-wires. c) Preoperative plan with trajectories (green) aligned to postoperative 3D models with generic cylindrical objects aligned to the postoperatively segmented trajectories (red). d) Planned and actual entry point visualized on the preoperative 3D models.

by aligning a generic cylindrical object to the segmented wire (see Figure 6c). The entry point was defined as the first point along the trajectory intersecting with the preoperative 3D model (see Figure 6d).

Primary outcome measures were the 3D angle between planned and executed trajectories as well as the 3D distance between planned and executed entry points. Secondary outcome measures for each vertebra included registration error and surface digitization time, the number of sampled points used for registration and the times for inserting each K-wire.

2.5 Implementation

The method was implemented as a holographic Universal Windows Platform (UWP) application using Unity (version 2017.4.9f1 Personal (64bit), Unity Technologies, San Francisco, CA, USA) and Microsoft Visual Studio (version Community 2017, Microsoft Corporation, Redmond, WA, USA). The code will be made available online: `card.balgrist.ch/holosurfacedigitization`. It was deployed to a Microsoft HoloLens on which the Windows 10 April 2018 Update (10.0.17134.80) operating system was running. The prototypes of the 3D printed parts were manufactured using a Formiga P100 3D printer (EOS GmbH Electro Optical Systems, Krailling, Germany) and made of biocompatible polyamide 2200.

3 Results

The evaluation of the primary outcome resulted in a mean error of $3.38 \pm 1.73^\circ$ for the trajectory orientation and 2.77 ± 1.46 mm for the entry point localization. Error distributions are visualized in Figure 7. The minimum and maximum trajectory errors were 1.16° and 6.33°, respectively. No outliers were observed with respect to the trajectory error. Extreme values of entry point errors were 0.71 mm and 7.20 mm, the latter being the only outlier.

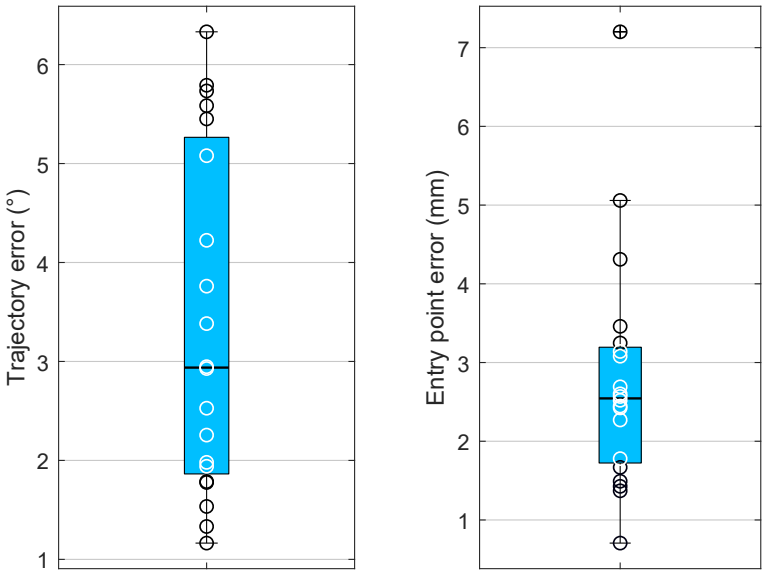

Fig. 7: Error distributions for trajectories (left) and entry points (right). Bold line: median, box: 25th-75th quantile, whiskers: $\pm 2.7\sigma$ (99.3%), crosses: outliers.

On average, the registration RMSE was 1.62±0.26 mm and it took the surgeon on average 125±27 s to digitize the bone surface, i.e. collect the points. Thereby, a mean of 1'983±404 points were collected per vertebra. Pearson product-moment correlation revealed that there was no relationship between the number of collected points and the registration RMSE (r = -0.06). The mean time needed for navigated insertion of one K-wire was 147±55 s. Thus, the duration of the entire workflow for one vertebra was 419 s on average. In five cases, the registration had to be repeated due to unspecified HoloLens OS failure. In one case, the surgeon decided that the registration was not good enough and restarted the application (L3, phantom 1).

4 Discussion

Various navigation approaches have been proposed for spinal surgery due to the high demands placed on precision and safety. However, none of the existing concepts has been established as a widely accepted clinical gold standard. An ideal navigation solution should be highly accurate, avoid radiation exposure, be cost- and time-effective, and simple in use and maintenance. In this study, we presented a radiation-free navigation approach for spinal fusion surgery comprising surface-based registration and intuitive holographic navigation. Our method has low requirements to computation and hardware. It can be implemented in an off-the-shelf OST-HMD, in our case the Microsoft HoloLens.

Several intraoperative surface digitization approaches that eliminate the need of intraoperative imaging have been evaluated in clinical settings [16–18]. They can be considered as very precise, if relying on expensive optical tracking devices. Nottmeier et al. [16] reported a mean registration error of 0.9 mm which is comparable to our RMSE of 1.62 mm on average. In terms of screw insertion accuracy, the results of Ma et al. [23] were similar (3.35 mm, 2.74°) to ours (2.77 mm, 3.38°) although a comprehensive high-end system was used. Due to these promising results with respect to accuracy, our low-cost navigation solution may have the potential for clinical use.

A different, yet very popular navigation method is 3D printing of patient-specific instruments (PSI) [9]. However, the main drawback of PSI systems are high production costs per case and long production time. Merc et al. [10] employed PSI in a randomized clinical trial to evaluate navigated pedicle screw placement accuracy in comparison to a control group where the fluoroscopy-controlled free-hand technique was used. For the lumbar segment, they reported a deviation of the entry point by 0.3 mm (interventional group) vs. 1.5 mm (control group) in the sagittal and 0.7 mm vs. 0.2 mm in the transversal plane. The sagittal and transversal deviations with respect to trajectory orientation were 1° vs. 6° and 1° vs 0°, respectively. Although differences were statistically significant for the sagittal comparisons, PSI navigation still showed a high standard deviation of the error.

Navigation methods are often criticized because their application can result in an increase of the surgery time. At least, the evaluation of the mean registration time in our study (125 s) was similar to state-of-the-art optical navigation system (117 s) [16]. PSI-navigated pedicle screw placement is faster than intraoperative surface digitization as the registration can be performed by placing the PSI on the bone surface. Farshad et al. reported an average time of 74 s for pedicle screw placement [9]. However, their study did not consider the time required to debride the bone from periosteum which is a necessary preparation step before PSI placement [38, 39].

Similar to our study, attempts have been made to develop simpler and more cost-effective techniques for navigation of pedicle screw insertion. Walti et al. [40] developed a small, custom-built device that relies on an inertial measurement unit. They conducted a preclinical cadaver study achieving an accuracy of 2.7° and 3.5° in the sagittal and axial plane, respectively. However, the approach lacked guidance of the screws' entry points and it provided registration only based on specific bony landmark points. Relying on the identification of specific bony landmarks is known to be error-prone. The study of Gibby et al. [41] evaluated the feasibility of the HoloLens for navigating a needle percutaneously to mimic pedicle screw placement. The target for needle placement was a lumbar spine phantom, wrapped in an opaque silicon block. Intraoperative registration was carried out using commercial software which then was refined manually by the user. The registration process was the main limitation of the study: It is based on intraoperative CT and the object to be registered needs to be simple and large, such as the silicon block.

This study has several limitations. The evaluation was performed on bone phantoms which did not include surrounding soft tissue structures. In a real surgery, such soft tissue structures could have a negative influence on the sampling process. However, we used specific bone regions for sampling that are known to be accessible in open surgery (see Figure 3). Other studies have also demonstrated that a similar registration accuracy can be achieved regardless whether phantoms or cadavers were used [23]. Furthermore, unlike in real surgery, the anatomy was rigidly attached to the table and thus could not move. For this reason, no motion compensation strategy was necessary, but it is known that Holograms are prone to drift once they have been placed [42]. Even though the surgeon tried to minimize head movement, drift may have negatively influenced our results. Finally, the proposed

method is partly constrained by current technical limitations of the HoloLens. It can be assumed that increased sensor quality in future releases will improve the accuracy of built-in tracking methods.

For future work, we plan to carry out a comprehensive cadaver evaluation on human specimen to evaluate clinical feasibility and surgical outcomes compared to the free-hand technique. The study shall include evaluation of subjective feedback on acceptance and usability by the performing surgeons. Furthermore, the intraoperative manual surface digitization quality on real anatomy needs to be assessed. Post-experimental analysis has also revealed that the sampling surfaces contained outliers not belonging to the actual bone surface. The precision of the registration may be further increased by developing an outlier removal strategy. Concluding, our preliminary evaluation indicates a precision which may be sufficient for clinical application.

Compliance with Ethical Standards

- Conflict of Interest: The authors declare that they have no conflict of interest.
- This article does not contain any studies with human participants or animals performed by any of the authors.
- This articles does not contain patient data.

References

1. Raciborski F, Gasik R, Kłak A (2016) Disorders of the spine. a major health and social problem. Reumatologia 54(4):196
2. Vos T, Flaxman AD, Naghavi M, Lozano R, Michaud C, Ezzati M, Shibuya K, Salomon JA, Abdalla S, Aboyans V, et al. (2012) Years lived with disability (ylds) for 1160 sequelae of 289 diseases and injuries 1990–2010: a systematic analysis for the global burden of disease study 2010. The lancet 380(9859):2163–2196
3. Van Tulder MW, Koes BW, Bouter LM (1997) Conservative treatment of acute and chronic nonspecific low back pain: a systematic review of randomized controlled trials of the most common interventions. Spine 22(18):2128–2156
4. Mirza SK, Deyo RA (2007) Systematic review of randomized trials comparing lumbar fusion surgery to nonoperative care for treatment of chronic back pain. Spine 32(7):816–823
5. Verlaan J, Diekerhof C, Buskens E, Van der Tweel I, Verbout A, Dhert W, Oner F (2004) Surgical treatment of traumatic fractures of the thoracic and lumbar spine: a systematic review of the literature on techniques, complications, and outcome. Spine 29(7):803–814
6. Maruyama T, Takeshita K (2008) Surgical treatment of scoliosis: a review of techniques currently applied. Scoliosis 3(1):6
7. Mason A, Paulsen R, Babuska JM, Rajpal S, Burneikiene S, Nelson EL, Villavicencio AT (2014) The accuracy of pedicle screw placement using intraoperative image guidance systems: A systematic review. Journal of Neurosurgery: Spine 20(2):196–203
8. Modi HN, Suh SW, Fernandez H, Yang JH, Song HR (2008) Accuracy and safety of pedicle screw placement in neuromuscular scoliosis with free-hand technique. European Spine Journal 17(12):1686–1696

9. Farshad M, Betz M, Farshad-Amacker NA, Moser M (2017) Accuracy of patient-specific template-guided vs. free-hand fluoroscopically controlled pedicle screw placement in the thoracic and lumbar spine: a randomized cadaveric study. European Spine Journal 26(3):738–749
10. Merc M, Drstvensek I, Vogrin M, Brajlih T, Recnik G (2013) A multi-level rapid prototyping drill guide template reduces the perforation risk of pedicle screw placement in the lumbar and sacral spine. Archives of orthopaedic and trauma surgery 133(7):893–899
11. Kantelhardt SR, Martinez R, Baerwinkel S, Burger R, Giese A, Rohde V (2011) Perioperative course and accuracy of screw positioning in conventional, open robotic-guided and percutaneous robotic-guided, pedicle screw placement. European Spine Journal 20(6):860–868
12. Tian NF, Huang QS, Zhou P, Zhou Y, Wu RK, Lou Y, Xu HZ (2011) Pedicle screw insertion accuracy with different assisted methods: a systematic review and meta-analysis of comparative studies. European Spine Journal 20(6):846–859
13. Narain AS, Hijji FY, Yom KH, Kudaravalli KT, Haws BE, Singh K (2017) Radiation exposure and reduction in the operating room: Perspectives and future directions in spine surgery. World journal of orthopedics 8(7):524
14. Gebhard FT, Kraus MD, Schneider E, Liener UC, Kinzl L, Arand M (2006) Does computer-assisted spine surgery reduce intraoperative radiation doses? Spine 31(17):2024–2027
15. Slomczykowski M, Roberto M, Schneeberger P, Ozdoba C, Vock P (1999) Radiation dose for pedicle screw insertion: fluoroscopic method versus computer-assisted surgery. Spine 24(10):975–983
16. Nottmeier EW, Crosby TL (2007) Timing of paired points and surface matching registration in three-dimensional (3d) image-guided spinal surgery. Clinical Spine Surgery 20(4):268–270
17. Richter M, Cakir B, Schmidt R (2005) Cervical pedicle screws: conventional versus computer-assisted placement of cannulated screws. Spine 30(20):2280–2287
18. Chiang CF, Tsai TT, Chen LH, Lai PL, Fu TS, Niu CC, Chen WJ (2012) Computed tomography-based navigation-assisted pedicle screw insertion for thoracic and lumbar spine fractures. Chang Gung Med J 35(4):332–8
19. Qian L, Unberath M, Yu K, Fuerst B, Johnson A, Navab N, Osgood G (2017) Towards virtual monitors for image guided interventions-real-time streaming to optical see-through head-mounted displays. arXiv preprint arXiv:171000808
20. Andress S, Johnson A, Unberath M, Winkler AF, Yu K, Fotouhi J, Weidert S, Osgood G, Navab N (2018) On-the-fly augmented reality for orthopedic surgery using a multimodal fiducial. Journal of Medical Imaging 5(2):021209
21. Sielhorst T, Feuerstein M, Navab N (2008) Advanced medical displays: A literature review of augmented reality. Journal of Display Technology 4(4):451–467
22. Navab N, Blum T, Wang L, Okur A, Wendler T (2012) First deployments of augmented reality in operating rooms. Computer 45(7):48–55
23. Ma L, Zhao Z, Chen F, Zhang B, Fu L, Liao H (2017) Augmented reality surgical navigation with ultrasound-assisted registration for pedicle screw placement: a pilot study. International journal of computer assisted radiology and surgery 12(12):2205–2215
24. Microsoft (2018) HoloLens Research mode. https://docs.microsoft.com/en-us/windows/mixed-reality/research-mode. Accessed 2018-11-01

25. Olson E (2011) Apriltag: A robust and flexible visual fiducial system. In: Robotics and Automation (ICRA), 2011 IEEE International Conference on, IEEE, pp 3400–3407
26. Wang J, Olson E (2016) Apriltag 2: Efficient and robust fiducial detection. In: IROS, pp 4193–4198
27. Microsoft (2018) Locatable camera. https://docs.microsoft.com/en-us/windows/mixed-reality/locatable-camera. Accessed 2018-11-05
28. Garrido-Jurado S, Muñoz-Salinas R, Madrid-Cuevas FJ, Marín-Jiménez MJ (2014) Automatic generation and detection of highly reliable fiducial markers under occlusion. Pattern Recognition 47(6):2280–2292
29. Garrido-Jurado S, Munoz-Salinas R, Madrid-Cuevas FJ, Medina-Carnicer R (2016) Generation of fiducial marker dictionaries using mixed integer linear programming. Pattern Recognition 51:481–491
30. Romero-Ramirez FJ, Muñoz-Salinas R, Medina-Carnicer R (2018) Speeded up detection of squared fiducial markers. Image and Vision Computing
31. Kalman RE (1960) A new approach to linear filtering and prediction problems. Journal of basic Engineering 82(1):35–45
32. Bradski G, Kaehler A (2000) Opencv. Dr Dobb's journal of software tools 3
33. Horn BK (1987) Closed-form solution of absolute orientation using unit quaternions. JOSA A 4(4):629–642
34. Microsoft (2017) Use the HoloLens clicker. https://support.microsoft.com/de-ch/help/12646/hololens-use-the-hololens-clicker. Accessed 2018-11-03
35. Microsoft (2018) HoloToolkit 2017.4.1.0. https://github.com/Microsoft/MixedRealityToolkit-Unity/releases/tag/2017.4.1.0. Accessed 2018-11-03
36. Besl PJ, McKay ND (1992) Method for registration of 3-d shapes. In: Sensor Fusion IV: Control Paradigms and Data Structures, International Society for Optics and Photonics, vol 1611, pp 586–607
37. Pearson K (1901) Liii. on lines and planes of closest fit to systems of points in space. The London, Edinburgh, and Dublin Philosophical Magazine and Journal of Science 2(11):559–572
38. Schweizer A, Mauler F, Vlachopoulos L, Nagy L, Fürnstahl P (2016) Computer-assisted 3-dimensional reconstructions of scaphoid fractures and nonunions with and without the use of patient-specific guides: early clinical outcomes and postoperative assessments of reconstruction accuracy. The Journal of hand surgery 41(1):59–69
39. Roner S, Vlachopoulos L, Nagy L, Schweizer A, Fürnstahl P (2017) Accuracy and early clinical outcome of 3-dimensional planned and guided single-cut osteotomies of malunited forearm bones. The Journal of hand surgery 42(12):1031–e1
40. Walti J, Jost GF, Cattin PC (2014) A new cost-effective approach to pedicular screw placement. In: Workshop on Augmented Environments for Computer-Assisted Interventions, Springer, pp 90–97
41. Gibby JT, Swenson SA, Cvetko S, Rao R, Javan R (2018) Head-mounted display augmented reality to guide pedicle screw placement utilizing computed tomography. International Journal of Computer Assisted Radiology and Surgery pp 1–11
42. Vassallo R, Rankin A, Chen EC, Peters TM (2017) Hologram stability evaluation for microsoft hololens. In: Medical Imaging 2017: Image Perception, Observer Performance, and Technology Assessment, International Society for Optics and Photonics, vol 10136, p 1013614